Holographic acoustic tweezers

Asier Marzo[a,b,1] and Bruce W. Drinkwater[a]

[a]Faculty of Engineering, University of Bristol, BS8 1TR Bristol, United Kingdom; and [b]UpnaLab, Universidad Pública de Navarra, Campus Arrosadia, 31006 Pamplona, Spain

Acoustic tweezers use sound radiation forces to manipulate matter without contact. They provide unique characteristics compared with the more established optical tweezers, such as higher trapping forces per unit input power and the ability to manipulate objects from the micrometer to the centimeter scale. They also enable the trapping of a wide range of sample materials in various media. A dramatic advancement in optical tweezers was the development of holographic optical tweezers (HOT) which enabled the independent manipulation of multiple particles leading to applications such as the assembly of 3D microstructures and the probing of soft matter. Now, 20 years after the development of HOT, we present the realization of holographic acoustic tweezers (HAT). We experimentally demonstrate a 40-kHz airborne HAT system implemented using two 256-emitter phased arrays and manipulate individually up to 25 millimetric particles simultaneously. We show that the maximum trapping forces are achieved once the emitting array satisfies Nyquist sampling and an emission phase discretization below $\pi/8$ radians. When considered on the scale of a wavelength, HAT provides similar manipulation capabilities as HOT while retaining its unique characteristics. The examples shown here suggest the future use of HAT for novel forms of displays in which the objects are made of physical levitating voxels, assembly processes in the micrometer and millimetric scale, as well as positioning and orientation of multiple objects which could lead to biomedical applications.

acoustic tweezers | contactless manipulation | acoustic levitation | acoustophoresis | displays

In 1986, Ashkin et al. (1) showed that dielectric particles can be trapped in a focused laser beam and that this principle also works for bacteria as well as viruses (2). Since then, optical tweezers have become a fundamental tool in biology and physics, leading to the measurement of the DNA spring constant (3), transport of Bose–Einstein condensates (4, 5), and trapping of cold atoms (6). Holographic optical tweezers (HOT) (7–10) further extended this functionality to enable the simultaneous manipulation of multiple particles resulting in applications such as the assembly of 3D colloidal structures (11), quasicrystals (12, 13), and nanowires (14) as well as the probing of soft matter (15).

Acoustic tweezers use the radiation forces exerted by ultrasonic waves to trap particles (16–18) ranging from less than 1 μm (19, 20) to more than 1 cm (21) in various media such as air (21), water (22), and potentially (only proven theoretically) in biological tissue phantoms (23, 24). Acoustic radiation forces are five orders of magnitude higher per unit input power than in optical trapping, giving them a significant efficiency advantage and enabling low-power operation which is critical in cell manipulation applications (25). Consequently, acoustic tweezers are becoming a fundamental tool for disease diagnosis (26), laboratory-on-a-chip manipulation (27), centimeter-scale containerless processing (21, 28), and in vivo applications such as the manipulation of kidney stones (29).

Recent advances have enabled the dynamic positioning of acoustically trapped particles in one- (28), two- (21), and three dimensions (30–32); however, the particles were moved as a group, with no individual particle control. Acoustic radiation force devices using 3D printed lenses have also been used to produce complex patterns of particles (33), but these patterns were static and 2D. Similarly, by multiplexing a focal point it was possible to manipulate in midair two droplets of water in 2D (34). To date, the most versatile dynamic device enables two particles to be manipulated independently in 2D using a ring of emitters in a microfluidic chamber (22).

Being able to individually control many particles with the versatility and efficiency of acoustic tweezers would enable many new applications such as display spaces where levitated physical voxels form objects in 3D, or fabrication of structures ranging from the microscale for tissue engineering to the centimeter scale for placement of integrated circuits. Also, the inherent capability of ultrasound to act through tissue would permit the use of holographic acoustic tweezers (HAT) for complex in vivo procedures in which trapped particles assume different manipulation roles, e.g., hold, orientate, release, bring together, or separate.

In this paper, we explore the capabilities of HAT to dynamically manipulate multiple particles simultaneously in midair. We describe and evaluate an algorithm that enables the realization of HAT by controlling the emitted field from ultrasonic phased arrays. For optical tweezers, the digital light modulator (DLM) was revolutionary as it provided more than 500×500 pixels of phase control (7). Acoustic lenses have recently been exploited to apply similar high-resolution phase modulation (33), but they are static and thus not suitable for dynamic HAT. Phased arrays are the current dynamic acoustic emitter that offers the best potential solution, e.g., emitters of up to 50×50 elements have been described in the literature (35); however, this acoustic array contains two orders of magnitude fewer elements than commonly available DLMs. We show that despite this reduced element count, it is possible to realize an HAT with independent manipulation capabilities similar to those achieved in HOT.

Significance

Holographic optical tweezers use focused light to manipulate multiple objects independently without contact. They are used in tasks such as measuring the spring constant of DNA, the pulling force of the kinesin protein, or to trap matter in exotic states. Differently, acoustic tweezers use sound radiation forces to trap particles at a larger scale (i.e., from micrometers to centimeters). However, previous implementations did not provide individual control. We present the realization of holographic acoustic tweezers. Using an array of sound emitters, we engineer the generated sound field to manipulate multiple particles individually. This enables applications in contactless assembly both at the micrometer and centimeter scale as well as the creation of displays in which the pixels are levitating particles.

An algorithm capable of realizing HAT is distinctly different from those used previously for HOT. In optics, a focus on the particle is sufficient for trapping (36) whereas in acoustics, only negative contrast particles (i.e., the acoustic impedance of the particle is less than that of the medium) will be trapped in this way (37). However, acoustic trapping in air and most particles in water-based media lead to positive acoustic contrast particles. Therefore, in practice, acoustic trapping is only achieved at the zero-pressure regions of standing-wave nodes (28), focused vortices (38), twin traps (31), or bottle beams (31).

Here, we describe an iterative backpropagation (IB) algorithm that we use to calculate the emission phases of the array elements to realize a functional HAT. This algorithm uses a modified version of the iterative angular spectrum approach (33) (IASA); IASA is itself based on the Gerchberg–Saxton (GS) algorithm (39). Differently from IASA and GS, IB uses propagators derived from a specific transducer model which enables us to accurately predict the acoustic field with minimum computational effort. In addition, IB permits the creation of focal points as well as the enforcement of phase dependencies between these points, allowing us to efficiently generate different traps (i.e., focal points, twin traps, and vortices) at arbitrary positions.

We show that HAT can be realized using this algorithm and two 256-emitter arrays with an element spacing and diameter of 1.2λ (1 cm) operating at 40 kHz with a phase resolution of π/16 radians and an update rate of 90 frames per second. For in-plane 2D manipulation we used a single array placed 15.1λ (13 cm) above a sound-reflective surface; for 3D manipulation we used two opposed arrays separated by 26.7λ (23 cm) (*SI Appendix*, Fig. S1). These separations were selected to provide high acoustic pressure in the desired planar or volumetric manipulation region (*SI Appendix*, Fig. S2). We use these systems to demonstrate the controlled manipulation of multiple expanded polystyrene (EPS) spheres (1–3-mm diameter) (Movie S1).

Results

In-Plane Manipulation. The multiparticle manipulation capabilities of HOTs are usually demonstrated with the control of various particles in a single plane (7). Here, we realize an in-plane HAT with the particles initially resting on a reflective surface. This is a common practical scenario, e.g., with particles resting on a microscope cover slide (40). If a sound beam is focused on a particle situated on a reflective surface, due to the interference between the incoming and reflected field, a local standing wave is created with the first node positioned λ/4 above the surface (Fig. 1). At this node, the forces in all three dimensions converge, which is the requirement for stable trapping. Thus, for particles
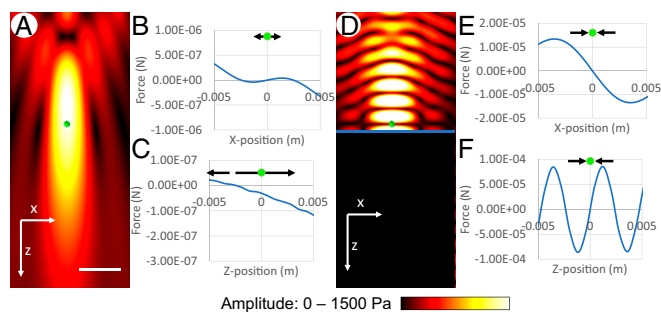
located on a planar reflective surface, HAT can be realized by focusing the array on the particles and manipulating these foci.

Multiple particles are manipulated by generating multiple foci, causing the particles to be trapped in the nodes formed just above the reflector. The IB algorithm (*Materials and Methods*) is used to generate focal points at the positions of the particles and the emitter phases are dynamically controlled to move the foci and hence the particles. The application of the IB algorithm ensures that the pressure amplitudes at the foci are maximized and that the deviation between the various points is minimized, i.e., the normalized SD of the focal pressure amplitude is reduced by 30% compared with the noniterative method (*Materials and Methods*). In Fig. 2 and Movie S2, we show the manipulation of 10 particles in a plane λ/4 above a reflector.

The minimum distance achieved between the particles was ~1.3 cm (1.5λ) regardless of the number of trapping points (*SI Appendix*, Fig. S3). At smaller distances, the focal points merged together inhibiting independent control. The Rayleigh resolution limit (41) for this configuration is 0.85 cm (1.22λL/A, where L = 13 cm is the focal distance and A = 16 cm is the aperture), but this minimum distance between traps can only be obtained with smaller acoustic emitters; we show that the amplitude distribution of two close focal points depends on the pitch of the array in *SI Appendix*, Fig. S4.

Here, at excitation signals of 10 volts peak-to-peak (Vpp) (9.5 W of input power), we manipulated 12 particles (Fig. 2); and at 16 Vpp with double the number of transducers (57 W of input power), we manipulated 25 particles (Movie S3). In *SI Appendix*, Fig. S5, we show that when attempting to use our system to generate 28 traps, the generated undesired artifacts (secondary high-amplitude regions that were not defined as focal points) start to become as powerful as the traps. Therefore, for this system, further increase of the power will have no additional benefit in terms of the number of independent traps. The effect of artifacts is explored in more detail in *Discussion*.

Beyond Trapping: In-Plane Torque and Orientation. HOT have been used to create traps with different functionalities (7), for example vortices that can transfer orbital angular momentum (OAM). In acoustics, single-vortex beams have also been used to trap and transfer OAM (42–45). In HAT, we can generate multiple vortices with independent chirality using the IB algorithm, but this time tuned to create vortices. In Fig. 3 and Movie S4, we generate three vortices above a water surface and individually change their chirality in real time. The vortices were separated by 10λ to correctly observe the rotation of soap bubbles on the surface of the water. With our system, it was possible to bring two vortices cores within ~1.4 cm (1.6λ) (*SI Appendix*, Fig. S6) and generate up to five discernible vortices (*SI Appendix*, Fig. S7).

In the past, it has been shown that an acoustic twin trap can orientate asymmetric particles (21, 31). The IB algorithm presented in this paper (*Materials and Methods*) is capable of generating multiple twin traps at arbitrary positions and with different orientations. Twin traps and vortices can create converging forces along the direction of propagation (i.e., z axis); however, this force was not enough to levitate the particles since it can be more than 30× weaker than the lateral forces (46). Hence, we adopted a time-multiplexing approach between twin traps (to orientate) and focal points (to generate enough trapping force); this approach has been recently demonstrated for one particle (47) but here we show that it can be used for multiple particles to achieve independent control of particle orientation. In Fig. 4 and Movie S5, we show the orientation of four asymmetric particles and change their orientations individually by rotation of the twin traps. With our current configuration, it was possible to generate up to seven twin traps (*SI Appendix*, Fig. S8) with a minimum distance of ~1.4λ between them (*SI Appendix*, Fig. S9).

Fig. 1. Trapping over a reflective surface. (*A*) Pressure amplitude generated by an array focused at a single point in free space; (*D*) pressure amplitude when the same focal point reflects on a surface (blue line). Trapping forces in the x direction (*B* and *E*) and z direction (*C* and *F*) generated by the focal point. (*B* and *C*) Nonconverging forces without a reflector; (*E* and *F*) converging forces in the presence of a reflector. (Scale bar, *A*: 2 cm.) Particle is located at the origin.
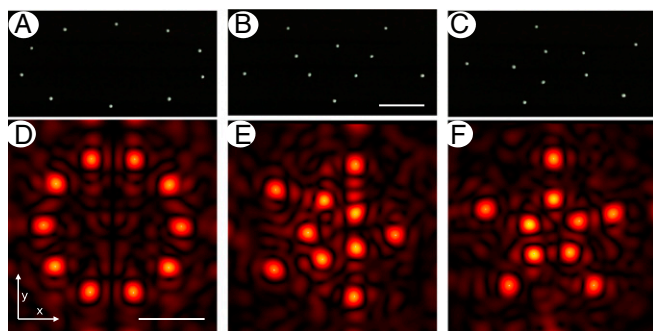
Fig. 2. Simultaneous in-plane manipulation of 10 EPS particles of 2-mm diameter. The particles are trapped 2.3 mm (λ/4) above a reflective surface. (*A*) The particles start in a circle, (*B*) odd particles move toward the center, and (*C*) the two concentric circles of particles rotate in opposite directions. (*D–F*) The simulated pressure-amplitude fields generated at the reflective surface. The 16 × 16 array was placed parallel to the surface 13 cm above it. (Scale bar, *B* and *D*: 2 cm.)

Three-Dimensional Manipulation. To realize a 3D HAT we used a double-sided arrangement made of two opposed arrays (16 × 16 emitters) separated by 26.7λ (23 cm) to create multiple standing waves with nodes located at the target trapping positions. To do so, the IB algorithm first creates high-intensity foci at the specified trapping positions. These foci are then all shifted vertically (in the z direction) by λ/2 by the application of an additional phase delay of π radians to the top array elements, thereby nodes now occur at the required trapping locations. Hence, the converging forces required for trapping are created and can be manipulated by dynamically moving the foci. In Fig. 5 and Movie S6 we show 12 particles that start in a single plane, then morph into an icosahedron that afterward rotates around different axes. In HOT, this same manipulation has been shown (48), albeit on a much smaller length scale.

In *SI Appendix*, Figs. S10 and S11, we use acoustic field simulations to show that the trapping forces decrease linearly with the number of trapped particles. More importantly, keeping the acoustic power per unit area constant and reducing the pitch of the emitters improves the performance of HAT in terms of trapping stiffness. However, we show that, once Nyquist sampling (49) is achieved (emitter pitch of λ/2), no further improvements can be obtained. The HAT presented in this paper has a transducer spacing of 1.2λ, thus it is somewhat suboptimal in this regard. We also use acoustic field simulations to show that trapping strength does not increase significantly for phase emission discretization levels below π/8 radians (*SI Appendix*, Fig. S12). Since our system discretizes phase at π/16 radians it is already optimal in that sense. We note that this is consistent with findings from single-trap systems where a phase discretization of π/5 was found to be sufficient (50).

Up to 27 particles have been manipulated in 3D using HOT (11). Despite our limited array size (i.e., 16 × 16 cm), spatial discretization (i.e., 16 × 16 elements), and pressure levels (i.e., 15 Vpp to generate 2.3 Pa at 1 m with each emitter), we achieved simultaneous dynamic manipulation of 12 particles (Fig. 5) and the partial manipulation of 25 particles (Movie S3). In the last case, some particles escaped the traps as they were being moved due to the increased trapping stiffness required to counteract the oscillations of the particles in air. Therefore, reaching the same number of particles as HOT would be feasible employing more powerful or smaller emitters.

Discussion

We quantified the quality of the traps using the stiffness (i.e., the spatial gradient of the force), which represents the converging

forces of the traps. From our simulations (*SI Appendix*, Fig. S10) and experiments (*SI Appendix*, Fig. S13) we observed that the trapping forces are inversely proportional to the number of generated traps. Simulations show that the stiffness can be improved by decreasing the pitch of the emitters (*SI Appendix*, Fig. S10) or by increasing the emission phase resolution (*SI Appendix*, Fig. S12). However, when close-packed emitting elements reach a pitch smaller than λ/2 and an emission phase resolution below π/8 no further improvement can be obtained.

The IB algorithm maximizes the trap quality (i.e., stiffness), rather than minimizing artifacts. As a result, artifacts are often present (e.g., Fig. 4 B and D and *SI Appendix*, Figs. S3 and S5). In general, for a low number of traps (i.e., <10) the traps have significantly larger pressure amplitude than these artifacts and thus more trapping force, so they do not cause a significant problem. However, as the number of traps increases, their trapping forces decrease, and the artifacts become increasingly powerful; this is shown qualitatively in *SI Appendix*, Fig. S5 and quantitatively in *SI Appendix*, Fig. S14. We note that with the future possibility of ultrasonic arrays with more transducers and a smaller pitch it may be possible to develop algorithms that maximize trap stiffness and also minimize artifacts.

The appearance of artifacts and ghost traps is a very pressing problem in HOT (51); this problem also appears in our HAT system. On the one hand, secondary nodes appear along the z axis. The focal points are inherently elongated along the direction of propagation (i.e., in an ellipsoidal shape) and this creates multiple secondary nodes separated by λ/2. The length of the focal zone (or Rayleigh length) depends on the wavelength, aperture of the array, and distance from the array. In *SI Appendix*, Fig. S15, we show the amplitude profile of focal zones for our system depending on the number of transducers and traps; the Rayleigh length is similar for all cases (i.e., 7 cm ∼ 8 nodes). We note that stronger focusing (i.e., lower F#) can be used to reduce the length of the focal zone and thus reduce the number of secondary nodes.

Undesired secondary traps can also be created in the XY plane, for example a focus at a single point can create secondary areas of high intensity outside of the focal area following an Airy amplitude distribution (52). When our phased array generates multiple focal points, it produces several of these secondary focal points (also called artifacts or ghost traps). In *SI Appendix*, Fig. S14 we show how the ratio between the minimum amplitude of
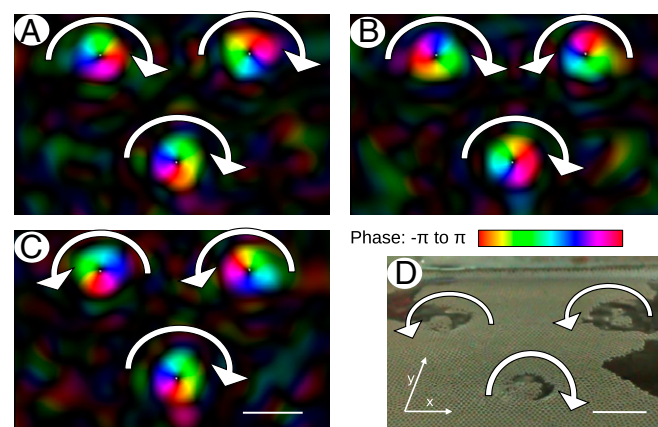

Fig. 3. Generation of vortices with independent chirality. (*A–C*) Simulated phase profile on a plane parallel to an array placed 15.1 λ (13 cm) above it. (*A*) All of the vortices are clockwise. (*B*) The top right vortex has changed to counterclockwise. (*C*) The top-left vortex has also changed to counterclockwise. (*D*) Bubbles on the surface of a water tank rotate according to the direction of the vortices from *C*. (Scale bar, *C* and *D*: 2 cm.)
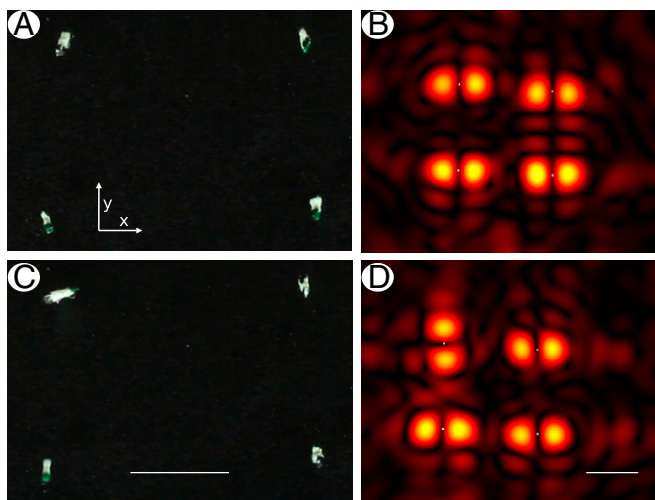
Marzo and Drinkwater

Fig. 4. Individual orientation of asymmetric particles trapped above a reflective surface with an array placed 15.1 λ (13 cm) above it. (*A*) All EPS particles aligned along the *y* axis; (*C*) one EPS particle is orientated along the *x* axis. (*B* and *D*) Corresponding simulated pressure amplitude at the reflecting surface. (Scale bar, *C* and *D*: 2 cm.)

the focal points and the maximum amplitude of the artifacts varies with the number of traps. As mentioned before, the traps are significantly stronger than the artifacts for relatively small numbers of traps (i.e., <10) but, as the number of traps increase, their strength reduces until they approach that of the artifacts. For the 16 × 16-element array used here, the ratio is 16:1 for one focal point and decreases to 3:1 for 25 traps. Surprisingly, emitters with finer pitch lead to stronger artifacts (*SI Appendix,* Fig. S16 *A* and *B*) but have the advantage of generating the secondary lobes further away from the central region (*SI Appendix,* Fig. S16 *C* and *D*).

A trapped particle will scatter sound and affect nearby particles. However, for the particles used here (i.e., 1–2-mm diameter) this effect was small. Movie S7 shows that particles of 1–2-mm diameter do not affect the particles in the nodes above or below in a perceivable way. In *SI Appendix,* Fig. S17 we show a simulation of how particles of different diameters affect the nearby acoustic field, e.g., nodes are only displaced by 0.12 mm when a 1-mm diameter particle is added in the next node, this distortion becomes more pronounced as the particle size increases.

The Rayleigh criterion (41) determines how close two focal points can be generated without getting too distorted (e.g., start to merge), hence we considered it to be an adequate indicator of the minimum lateral distance between the traps. In our setup, this minimum distance between traps was 1.4λ which is several times larger than the particle size.

The repositioning accuracy of the particles was ±0.1 mm (λ/86) for the in-plane and ±0.5 mm (λ/17) for the 3D manipulation. Similar levels (relative to the wavelength) of positional deviations occur in optical trapping, where the particle center is not always at a constant distance to center of the focus (7). The trapped particles showed good stability over time; in Movie S8 a time lapse of 1 h showed no noticeable deviation apart from that induced from air currents.

Optically trapped particles are often used as handles to manipulate other samples [such as DNA strands (2)]. Similarly, we attached EPS spheres to different objects and manipulate these handles, e.g., to post a thread through a hole in a piece of fabric (Movie S1).

The demonstrated system operates in air with a wavelength of 8.6 mm but, in principle, HAT can be scaled down by increasing the frequency and applied to other propagation media. For instance, a system operating at 7.5 MHz in water-based solutions would have a wavelength of 200 um, enabling the trapping of 20-um cells (the current HAT can trap particles smaller than λ/10). The demonstrated 3D HAT employed two arrays of 256 elements, with future systems containing more and smaller elements, or higher emitter output pressure, improved capabilities can be expected. In the medical domain, arrays with twice the number of elements are already available (53). Similarly, capacitive micromachined ultrasonic transducers will enable the miniaturization of the systems for working at the microscale wavelength (54).

Larger systems would enable the trapping of more particles, thus allowing the creation of displays made of levitated physical voxels, these displays would have characteristics that no existing display provides. Holograms can only be viewed from specific angles and both volumetric displays or the recent photophoretic displays are based on light reflection, so they can only operate under specific lighting conditions (55).

In *SI Appendix, Materials and Methods* we describe the manual and semiautomatic approaches employed to load the particles into the system. We note that a combination of HAT with tracking methods would enable an automatic solution for inserting the particles. For example, a 3D tracking system could detect the position of the particles so that the traps are directly created at those positions.

We have presented a demonstration of HAT that enables the individual positioning of multiple particles in 2D and 3D. These results have come 20 years after the appearance of its optical analog (i.e., HOT). The IB algorithm was the key that unlocked the realization of HAT. It allowed us to create multiple functional traps using arbitrary arrangements of transducers. HAT enables the control of multiple particles individually with the unique advantages of acoustic radiation forces, i.e., scales from micro- to centimeters, support of multiple materials for samples and propagation media, and high ratio of input power to forces.

Materials and Methods

Hardware. We employed arrays of 16 × 16 1-cm diameter 40-kHz ultrasonic transducers (Murata MA40S4S) operating in air. An FPGA (Altera Cyclone IV EP4CE6) receives the phases to be emitted from the computer using UART protocol operating at 250 kbauds. Metal-oxide-semiconductor field-effect transistor (Mosfet) drivers (Microchip MIC4127) amplify the signals up to 15 Vpp half-square waves, which are fed into the transducers. Due to the narrowband nature of the transducers the output pressure was sinusoidal (50). This hardware had a phase-emission resolution of π/16 radians and
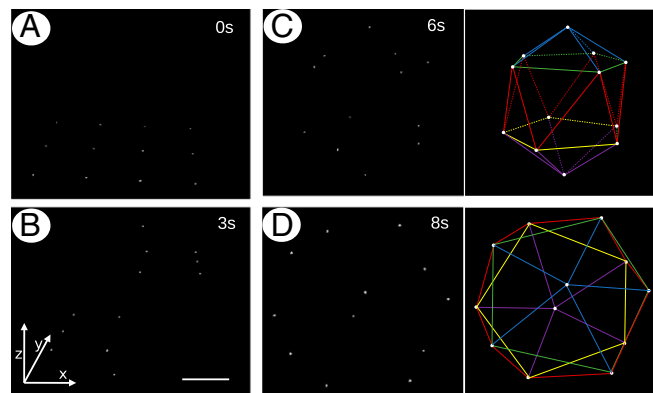

Fig. 5. Simultaneous manipulation of 12 particles starting in a planar grid which are morphed into a 3D icosahedron. (*A*) The particles start in a single plane as a 3 × 4 grid. (*B*) The particles are moved toward their target *z* positions. (*C*) The particles move to form an icosahedron. (*D*) The icosahedron is rotated 45° towards the viewer. For *C* and *D* the vertices of the icosahedron have been overlaid. (Scale bar, *B*: 2 cm.)

updated 90 times per second. The employed particles were EPS spheres of 1–3-mm diameter.

Algorithm for the HAT Calculation: IB. To generate multiple traps, we employed IB, which is a modification of the iterative IASA (33) and GS (39) algorithms. If we have n target traps at positions $t_1, \ldots, t_n$ we will split them into multiple control points depending on the desired type of trap. All of the resulting control points $c_1, .., c_k$ will have positions t_j, amplitudes a_j, and phases φ_j, where j is between 1 and k. Amplitude and phase are represented as a single complex number c_j. The position, amplitude, and phase of the control points depend on the type of trap to be generated and are described in the next paragraph. The amplitude associated with a given control point is $n_j = 1/m$, where m is the number of control points used to define a given trap. The phase of the control points starts at 0 radians but it is updated with every iteration of the algorithm. Only the phase of the first control point of a trap (φ_j) is updated; the rest of the points have a fixed phase relative to this first point and this phase pattern depends on the type of trap.

The shape of the three pressure-field shapes used to create the traps (i.e., focus, twin trap, and vortex) were found to be almost spatially invariant within the manipulation regions (*SI Appendix*, Fig. S18) This allowed us to identify a small number of features (or control points) that characterized each of these trap geometries. A focal point requires a single control point with the same position as the focus and unity amplitude. A twin trap has control points with a separation of 1.4λ between them; the control points can be rotated around the center of the trap to control its orientation. A vortex trap is decomposed into eight control points with the phase pattern following an increase from 0 to 2π radians in the counterclockwise or clockwise direction depending on the desired chirality of the vortex; the distance between these points and the center of the trap is 1.4λ. The location and phases of control points in various traps can be seen in *SI Appendix*, Fig. S19.

Consider a transducer l emitting with an amplitude a_l and phase φ_l (i.e., $p_l = a_l e^{i\varphi_l}$), to produce a complex field at r given by $p_{lr} = p_l h_{lr}$, where h_{lr} is the complex propagator from the position of transducer l to the point r; we precalculate the propagators from each transducer to each control point h_{lj}. We obtain this propagator using the far-field piston source model and setting the initial phase of the transducer to 0 (*SI Appendix, Materials and Methods*). The algorithm then proceeds by iteratively finding the phases for the transducers required to generate the target fields at the control points. If the phase variation between successive iterations is below a certain threshold (0.01 radians in our case) the algorithm stops; for the examples presented in the paper convergence was achieved after 200 iterations.

i) Forward propagate the transducer's complex pressure to the control points. $c_j = \sum p_l h_{lj}$.
ii) Normalize the amplitude at the control points and set the phase. $c_j = n_j c_j / |c_j|$, where n_j is the relative amplitude for the point j. For all of the points m which are not the first point of the trap, the phase is set in relation to the first point.
iii) Time reverse the control points into the transducers. $p_l = \sum c_j \overline{h_{lj}}$, where $\overline{h_{lj}}$ is the conjugate of the complex propagator.
iv) Normalize the output amplitude of the transducers: $p_l = p_l / |p_l|$.

This algorithm supports the generation of focal points, twin traps, and vortices at the target positions. Furthermore, the angle of the twin trap or the direction of the vortex is tunable by the user via the definition of the control points.

Using the above IB algorithm alone was sufficient for in-plane manipulations. However, for generating the nodes required for 3D manipulation, an additional step was used. First, as with 2D trapping, the IB algorithm is used to generate focal points at the trapping positions. Second, a π-radians offset is added to all elements in the top array to shift the high-intensity focus (i.e., an antinode) so that nodes are located at the target positions (*SI Appendix*, Fig. S20).

Using a direct time-reversal method (i.e., IB with one iteration) provided similar results in terms of mean force magnitudes (*SI Appendix*, Fig. S21) but the variation between traps was larger (*SI Appendix*, Fig. S22). A brute-force global maximization of the Gor'kov Laplacian (trapping stiffness) for all of the traps as an extension to Marzo et al. (31) algorithm did not produce functional traps.

1. Ashkin A, Dziedzic JM, Bjorkholm JE, Chu S (1986) Observation of a single-beam gradient force optical trap for dielectric particles. *Opt Lett* 11:288–290.
2. Ashkin A, Dziedzic JM (1987) Optical trapping and manipulation of viruses and bacteria. *Science* 235:1517–1520.
3. Wang MD, Yin H, Landick R, Gelles J, Block SM (1997) Stretching DNA with optical tweezers. *Biophys J* 72:1335–1346.
4. Gustavson TL, et al. (2002) Transport of Bose-Einstein condensates with optical tweezers. *Phys Rev Lett* 88:020401.
5. Kozuma M, et al. (1999) Coherent splitting of Bose-Einstein condensed atoms with optically induced Bragg diffraction. *Phys Rev Lett* 82:871–875.
6. Ketterle W, Davis KB, Joffe MA, Martin A, Pritchard DE (1993) High densities of cold atoms in a dark spontaneous-force optical trap. *Phys Rev Lett* 70:2253–2256.
7. Curtis JE, Koss BA, Grier DG (2002) Dynamic holographic optical tweezers. *Opt Commun* 207:169–175.
8. Dholakia K, MacDonald M, Spalding G (2002) Optical tweezers: The next generation. *Phys World* 15:31–35.
9. Molloy JE, Padgett MJ (2002) Lights, action: Optical tweezers. *Contemp Phys* 43:241–258.
10. McGloin D (2006) Optical tweezers: 20 years on. *Philos Trans R Soc A* 364:3521–3537.
11. Sinclair G, et al. (2004) Assembly of 3-dimensional structures using programmable holographic optical tweezers. *Opt Express* 12:5475–5480.
12. Roichman Y, Grier D (2005) Holographic assembly of quasicrystalline photonic heterostructures. *Opt Express* 13:5434–5439.
13. Čižmár T, Romero LD, Dholakia K, Andrews DL (2010) Multiple optical trapping and binding: New routes to self-assembly. *J Phys At Mol Opt Phys* 43:102001.
14. Agarwal R, et al. (2005) Manipulation and assembly of nanowires with holographic optical traps. *Opt Express* 13:8906–8912.
15. Phillips DB, et al. (2011) Surface imaging using holographic optical tweezers. *Nanotechnology* 22:285503.
16. Wu JR (1991) Acoustical tweezers. *J Acoust Soc Am* 89:2140–2143.
17. Brandt EH (2001) Acoustic physics. Suspended by sound. *Nature* 413:474–475.
18. Bruus H (2012) Acoustofluidics 7: The acoustic radiation force on small particles. *Lab Chip* 12:1014–1021.
19. Lam KH, et al. (2013) Ultrahigh frequency lensless ultrasonic transducers for acoustic tweezers application. *Biotechnol Bioeng* 110:881–886.
20. Lee J, et al. (2009) Single beam acoustic trapping. *Appl Phys Lett* 95:73701.
21. Foresti D, Poulikakos D (2014) Acoustophoretic contactless elevation, orbital transport and spinning of matter in air. *Phys Rev Lett* 112:024301.
22. Courtney CR, et al. (2014) Independent trapping and manipulation of microparticles using dexterous acoustic tweezers. *Appl Phys Lett* 104:154103.
23. Kang ST, Yeh CK (2010) Potential-well model in acoustic tweezers. *IEEE Trans Ultrason Ferroelectr Freq Control* 57:1451–1459.
24. Li Y, Lee C, Chen R, Zhou Q, Shung KK (2014) A feasibility study of *in vivo* applications of single beam acoustic tweezers. *Appl Phys Lett* 105:173701.
25. Riaud A, Baudoin M, Matar OB, Becerra L, Thomas JL (2017) Selective manipulation of microscopic particles with precursor swirling Rayleigh waves. *Phys Rev Appl* 7:024007.
26. Laurell T, Petersson F, Nilsson A (2007) Chip integrated strategies for acoustic separation and manipulation of cells and particles. *Chem Soc Rev* 36:492–506.
27. Ding X, et al. (2012) On-chip manipulation of single microparticles, cells, and organisms using surface acoustic waves. *Proc Natl Acad Sci USA* 109:11105–11109.
28. Whymark RR (1975) Acoustic field positioning for containerless processing. *Ultrasonics* 13:251–261.
29. Maxwell AD, et al. (2016) Vortex beams and radiation torque for kidney stone management. *J Acoust Soc Am* 139:2040.
30. Hoshi T, Ochiai Y, Rekimoto J (2014) Three-dimensional noncontact manipulation by opposite ultrasonic phased arrays. *Jpn J Appl Phys* 53:07KE07.
31. Marzo A, et al. (2015) Holographic acoustic elements for manipulation of levitated objects. *Nat Commun* 6:8661.
32. Prisbrey M, Raeymaekers B (2018) Ultrasound noncontact particle manipulation of three-dimensional dynamic user-specified patterns of particles in air. *Phys Rev Appl* 10:034066.
33. Melde K, Mark AG, Qiu T, Fischer P (2016) Holograms for acoustics. *Nature* 537:518–522.
34. Watanabe A, Hasegawa K, Abe Y (2018) Contactless fluid manipulation in air: Droplet coalescence and active mixing by acoustic levitation. *Sci Rep* 8:10221.
35. Inoue S, et al. (2017) Acoustic macroscopic rigid body levitation by responsive boundary hologram. arXiv:1708.05988. Preprint, posted August 20, 2017.
36. Grier DG (2003) A revolution in optical manipulation. *Nature* 424:810–816.
37. Melde K, et al. (2018) Acoustic fabrication via the assembly and fusion of particles. *Adv Mater* 30:1704507.
38. Baresch D, Thomas JL, Marchiano R (2016) Observation of a single-beam gradient force acoustical trap for elastic particles: Acoustical tweezers. *Phys Rev Lett* 116:024301.
39. Gerchberg RW, Saxton WO (1972) A practical algorithm for the determination of the phase from image and diffraction plane pictures. *Optik (Stuttg)* 35:237–246.
40. Kim MG, et al. (2017) Label-free analysis of the characteristics of a single cell trapped by acoustic tweezers. *Sci Rep* 7:14092.
41. Rayleigh L (1879) XXXI. Investigations in optics, with special reference to the spectroscope. *London Edinburgh Dublin Philos Mag J Sci* 8:261–274.
42. Hefner BT, Marston PL (1999) An acoustical helicoidal wave transducer with applications for the alignment of ultrasonic and underwater systems. *J Acoust Soc Am* 106:3313–3316.

43. Skeldon KD, Wilson C, Edgar M, Padgett MJ (2008) An acoustic spanner and its associated rotational Doppler shift. *New J Phys* 10:013018.
44. Volke-Sepúlveda K, Santillán AO, Boullosa RR (2008) Transfer of angular momentum to matter from acoustical vortices in free space. *Phys Rev Lett* 100:024302.
45. Marzo A, Caleap M, Drinkwater BW (2018) Acoustic virtual vortices with tunable orbital angular momentum for trapping of mie particles. *Phys Rev Lett* 120: 044301.
46. Franklin A, Marzo A, Malkin R, Drinkwater BW (2017) Three-dimensional ultrasonic trapping of micro-particles in water with a simple and compact two-element transducer. *Appl Phys Lett* 111:094101.
47. Cox L, Croxford A, Drinkwater BW, Marzo A (2018) Acoustic lock: Position and orientation trapping of non-spherical sub-wavelength particles in mid-air using a single-axis acoustic levitator. *Appl Phys Lett* 113:054101.
48. Grier DG, Roichman Y (2006) Holographic optical trapping. *Appl Opt* 45:880–887.
49. Nyquist H (1928) Certain topics in telegraph transmission theory. *Trans Am Inst Electr Eng* 47:617–644.
50. Marzo A, Corkett T, Drinkwater BW (2018) Ultraino: An open phased-array system for narrowband airborne ultrasound transmission. *IEEE Trans Ultrason Ferroelectr Freq Control* 65:102–111.
51. Hesseling C, Woerdemann M, Hermerschmidt A, Denz C (2011) Controlling ghost traps in holographic optical tweezers. *Opt Lett* 36:3657–3659.
52. Airy GB (1835) On the diffraction of an object-glass with circular aperture. *Trans Cambridge Philos Soc* 5:283.
53. Waag RC, Fedewa RJ (2006) A ring transducer system for medical ultrasound research. *IEEE Trans Ultrason Ferroelectr Freq Control* 53:1707–1718.
54. Wygant IO, et al. (2008) Integration of 2D CMUT arrays with front-end electronics for volumetric ultrasound imaging. *IEEE Trans Ultrason Ferroelectr Freq Control* 55: 327–342.
55. Smalley DE, et al. (2018) A photophoretic-trap volumetric display. *Nature* 553:486–490.

ENGINEERING